Orographic Influences on a Great Salt Lake–Effect Snowstorm

TREVOR I. ALCOTT

National Weather Service, Western Region Headquarters, Salt Lake City, Utah

W. JAMES STEENBURGH

Department of Atmospheric Sciences, University of Utah, Salt Lake City, Utah

(Manuscript received 15 November 2012, in final form 1 February 2013)

ABSTRACT

Although several mountain ranges surround the Great Salt Lake (GSL) of northern Utah, the extent to which orography modifies GSL-effect precipitation remains largely unknown. Here the authors use observational and numerical modeling approaches to examine the influence of orography on the GSL-effect snowstorm of 27 October 2010, which generated 6–10 mm of precipitation (snow-water equivalent) in the Salt Lake Valley and up to 30 cm of snow in the Wasatch Mountains. The authors find that the primary orographic influences on the event are 1) foehnlike flow over the upstream orography that warms and dries the incipient low-level air mass and reduces precipitation coverage and intensity; 2) orographically forced convergence that extends downstream from the upstream orography, is enhanced by blocking windward of the Promontory Mountains, and affects the structure and evolution of the lake-effect precipitation band; and 3) blocking by the Wasatch and Oquirrh Mountains, which funnels the flow into the Salt Lake Valley, reinforces the thermally driven convergence generated by the GSL, and strongly enhances precipitation. The latter represents a synergistic interaction between lake and downstream orographic processes that is crucial for precipitation development, with a dramatic decrease in precipitation intensity and coverage evident in simulations in which either the lake or the orography are removed. These results help elucidate the spectrum of lake–orographic processes that contribute to lake-effect events and may be broadly applicable to other regions where lake effect precipitation occurs in proximity to complex terrain.

1. Introduction

The Great Salt Lake (GSL) Basin of northern Utah is one of several regions where orography affects lake-, sea-, and ocean-effect precipitation (hereafter referred to collectively as lake effect). Covering an area less than 1/10th the size of Lake Superior, the GSL is surrounded by mountain ranges that are much larger than the modest orography around the Laurentian Great Lakes, which are the subject of the majority of the lake-effect literature. With a few exceptions (e.g., Hjelmfelt 1992; Saito et al. 1996; Onton and Steenburgh 2001), comprehensive studies examining the role of orography in the evolution of lake effect are nearly absent from peer-reviewed literature. This work utilizes observations and numerical simulations to improve our understanding of how orography affects the initiation, morphology, and intensity of the GSL effect.

GSL-effect events occur several times per year and impact transportation along a densely populated urban corridor (Carpenter 1993; Steenburgh et al. 2000; Steenburgh 2003; Alcott et al. 2012; Yeager et al. 2013). They develop when a cold air mass moves over the relatively warm waters of the GSL, initiating or enhancing moist convection. On average, periods with GSL effect (which is sometimes concurrent with precipitation generated by non-lake-effect processes) account for up to 8.4% of the total cool-season (16 September–15 May) precipitation [snow-water equivalent (SWE)] in areas south and east of the GSL (Yeager et al. 2013). Most (all) of this precipitation falls as snow at valley (mountain) locations. Intense and long-duration events occur occasionally, including two during the 22–27 November 2001 "Hundred-Inch Storm" that together produced 107.4 mm of SWE at the Snowbird Snowpack Telemetry (SNOTEL) site in the Wasatch Mountains (Yeager et al. 2013).

Corresponding author address: Dr. Trevor I. Alcott, National Weather Service, Western Region Headquarters, 125 S. State St., Salt Lake City, UT 84103.
E-mail: trevor.alcott@noaa.gov

DOI: 10.1175/MWR-D-12-00328.1

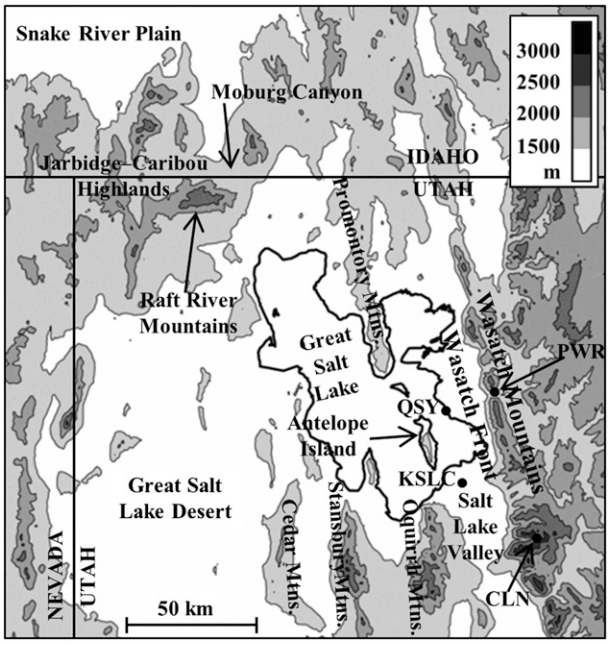

FIG. 1. Elevation (m, shaded, scale at top right) and landmarks of the study region.

The complex orography of northern Utah creates the potential for a variety of interactions between lake and orographic processes (Fig. 1). The GSL is bordered to the northwest by the Jarbidge–Caribou Highlands, to the east by the Wasatch Mountains, and to the south by the Cedar, Stansbury, and Oquirrh Mountains, all of which rise 1–2 km above lake level. The Promontory Mountains extend as a peninsula into the northern portion of the GSL, and a series of smaller barriers rise above the western shore, including the Hogup and Lakeside Mountains.

Northern Utah is one of many regions where lake effect interacts with complex terrain. Around the Laurentian Great Lakes, the modest rise in elevation from Lake Michigan to the hills of central Michigan has a minor, localized influence on lake-effect intensity (e.g., Hjelmfelt 1992). Hill (1971) found a 25–50-cm increase in mean annual snowfall for every 100-m increase in elevation above Lakes Erie and Ontario, including the Tug Hill plateau of northern New York. Laird et al. (2009) suggested that orography to the east and west of narrow Lake Champlain channels low-level flow and enhances overlake convergence during lake-effect events.

Beyond North America, lake effect occurs frequently in western Japan during the winter monsoon when cold, continental air from mainland Asia moves over the relatively warm waters of the Sea of Japan (Hozumi and Magono 1984). These events impact regions where high terrain lies close to the shoreline and contribute to a snowpack that contains up to 1620 mm of SWE in the mountains of the Hokuriku district (Matsuura et al. 2005). Sea of Japan snowstorms have been investigated through a variety of observational and numerical modeling approaches (e.g., Magono et al. 1966; Hozumi and Magono 1984; Saito et al. 1996; Kusunoki et al. 2004), with studies of orographic effects focused primarily on microphysical processes. Lake effect also occurs east and south of the Black Sea, where significant orographic barriers lie downstream in Georgia and Turkey (Kindap 2010; Markowski and Richardson 2010).

The situation around the Great Salt Lake is complicated by the presence of large orographic barriers surrounding the lake. Hence, we consider the effects of *upstream* and *downstream* barriers, located to the northwest and southeast of the GSL, respectively [based on the tendency for GSL-effect events to occur during northwesterly 700-hPa flow (Alcott et al. 2012)]. Although the role played by orography during GSL-effect events is not well understood, there is a wealth of peer-reviewed literature concerning orographic influences in northern Utah and other regions that provides valuable insight. Relevant concepts include 1) airmass transformation (e.g., Varney 1920; Sinclair 1994; Smith et al. 2003, 2005), 2) windward blocking and flow deflection (e.g., Mayr and McKee 1995; Colle et al. 2005; Cox et al. 2005), 3) orographically forced convergence (e.g., Mass 1981; Mass and Dempsey 1985; Chien and Mass 1997; Andretta and Hazen 1998), 4) orographic convection (Kirshbaum and Durran 2004, 2005a,b; Fuhrer and Schär 2005, 2007), and 5) thermally driven lake-mountain wind systems (e.g., McGowan et al. 1995; Stewart et al. 2002).

This paper explores the influence of upstream and downstream orographic features on the GSL-effect snowstorm of 27 October 2010 using radar, surface, and upper-air observations, gridded analyses, and numerical model simulations. We show that several orographic phenomena affect the evolution of the event and identify a synergistic interaction between lake and orographic processes that is crucial for the development of lake-effect precipitation. These results illustrate that orographic effects during lake-effect storms are not limited to upslope precipitation enhancement, with the orographic modification of the large-scale flow playing a primary role in the evolution of some lake-effect events.

2. Data and methods

a. Observational data and analyses

Surface observations were obtained from the MesoWest cooperative network (Horel et al. 2002) and

quality controlled using MesoWest data quality ratings (Splitt and Horel 1998), which compare observed station values to an objective analysis produced using multivariate linear regression. Observations deemed questionable by these ratings, or which failed subjective checks of temporal and spatial consistency, were not considered in our analysis. Upper-air soundings from the Salt Lake City International Airport (KSLC; see Fig. 1 for location) were retrieved from the University of Wyoming Department of Atmospheric Science. Promontory Point (KMTX) radar imagery comes from the National Climatic Data Center (NCDC) Next Generation Weather Radar (NEXRAD) archive in level III format (Crum et al. 1993). Operational North American Mesoscale Model (NAM) analyses were obtained from the National Oceanic and Atmospheric Administration (NOAA) National Operational Model Archive and Distribution System (NOMADS) at 12-km and 25-hPa horizontal and vertical grid spacing, respectively.

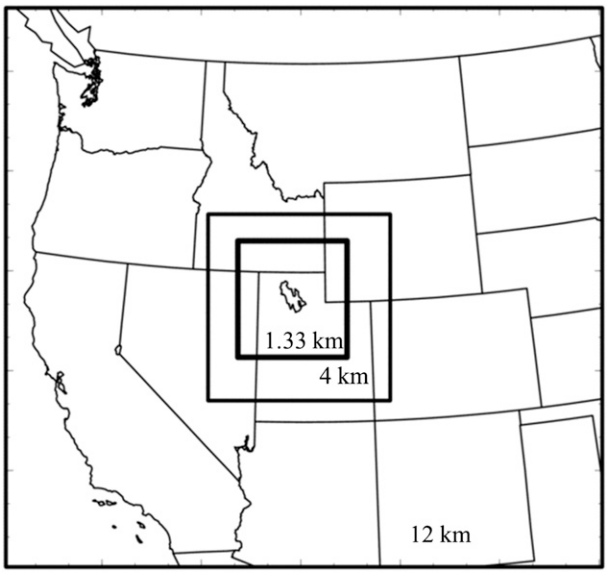

FIG. 2. WRF 12-, 4-, and 1.33-km domains.

b. Numerical model simulations

Numerical simulations were performed with the Weather Research and Forecasting Model, version 3.3.1 (WRF), which uses a nonhydrostatic, pressure-based, terrain-following η coordinate. All simulations use the Advanced Research WRF core and feature 3 one-way-nested domains with 35 vertical levels and horizontal grid spacings of 12, 4, and 1.33 km (Fig. 2). Only output from the 1.33-km domain is presented. All simulations use the Thompson et al. (2008) microphysics scheme, the Yonsei University planetary boundary layer scheme (Hong et al. 2006), the Rapid Radiative Transfer Model longwave and shortwave radiation schemes (Iacono et al. 2008), the Noah land surface model (Chen and Dudhia 2001), and the Kain–Fritsch 2 cumulus parameterization (Kain 2004). The convective parameterization is utilized only for the 12- and 4-km domains, while the other physics packages are applied to all three domains. Hydrometeor trajectories were calculated using average fall speeds weighted by the mixing ratios of each precipitation type.

NAM analyses provide the initial cold-start atmospheric and land surface conditions and lateral boundary conditions at 6-h intervals throughout the 24-h WRF simulations. Some modifications were made, however, to the initial conditions provided by the NAM to create more realistic land- and lake-surface analyses. Inspection of visible satellite imagery, SNOTEL data, and snow-cover analyses from the National Operational Hydrologic Remote Sensing Center (NOHRSC) showed that the NAM land surface analysis underestimated snow-cover extent and depth over northern Utah. Based on the NOHRSC and SNOTEL data, an approximate relationship between elevation and snowpack SWE was used to more accurately specify the initial snow cover and snow depth across the 1.33-km domain. Nonetheless, sensitivity to snow cover and snow depth is low, and simulations with no snow cover produced a precipitation distribution nearly identical to the control simulations. For the 4- and 12-km domains, the NAM snow analysis was deemed adequate. Based on satellite-derived skin temperature data from the Advanced Very High Resolution Radiometer (AVHRR), the NAM GSL temperature was too low. Therefore, we used the median, cloud-masked, AVHRR skin temperature over the GSL (13.3°C) from the most recent cloud-free overpass prior to the event to initialize the GSL temperature in all three domains. This temperature is within 0.5°C of the 0.4- and 1.4-m water temperatures observed by a U.S. Geological Survey (USGS) buoy in the center of the GSL. To account for the effects of salinity on latent heat fluxes, the surface layer parameterization was modified following Steenburgh and Onton (2001) to reduce saturation vapor pressure by 30% and 6% over the north and south arms of the GSL, respectively.

Our investigation uses a control simulation (CTL) followed by a series of sensitivity experiments involving modification of the terrain surrounding the GSL. CTL used orography generated by the WRF preprocessing system from the standard WRF 30-s terrain dataset. Terrain features were removed from the flat-no-lake (FLAT-NL), flat (FLAT), Wasatch Mountains (WAS), and downstream terrain (DT) simulations as shown in Fig. 3. The removal of terrain involved limiting the elevation of a specified area to 1280 m, the approximate

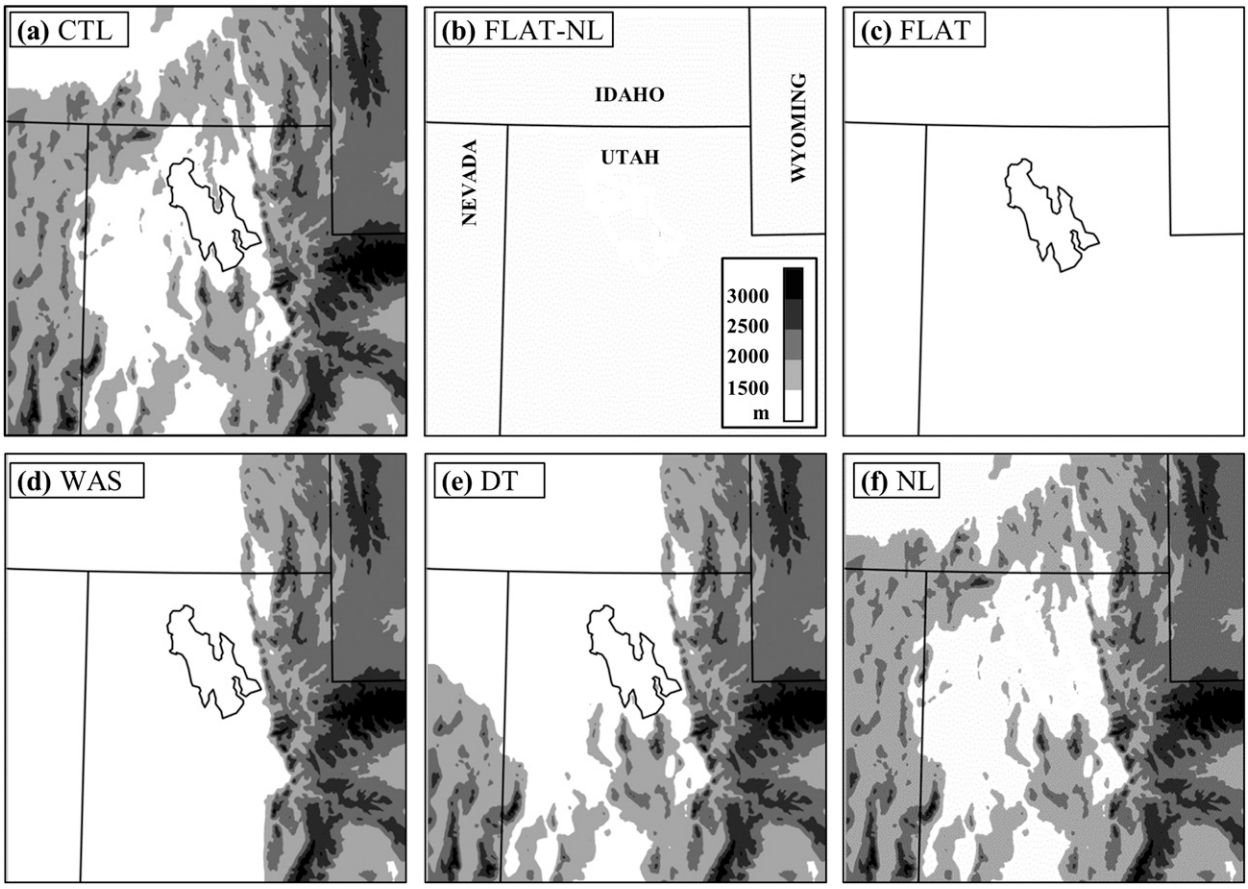

FIG. 3. WRF terrain elevations [m, shaded, scale in (b)] for the (a) CTL, (b) FLAT-NL, (c) FLAT, (d) WAS, (e) DT, and (f) NL simulations.

elevation of the GSL. Where terrain modification was performed in the 1.33-km domain, elevations in the parent 4-km domain were also reduced to 1280 m outward for an additional five grid points (20 km). Terrain was not modified in the outermost 12-km domain. Transition zones between real and modified terrain in both the 1.33- and 4-km domains were smoothed over a distance of 10 grid points to remove steep slopes.

Where terrain is modified, land surface characteristics such as land use, soil type, vegetation type, and vegetated fraction are retained. However, soil temperature, soil moisture, and land surface temperature are adjusted by the WRF preprocessing system using implicit relationships between these variables and elevation. Where the elevation of terrain is reduced to below the snow line, snow cover is automatically removed. The sensitivity to snow cover and land use is very low and we find it reasonable to attribute differences between CTL and the FLAT-NL, FLAT, WAS, and DT simulations to changes in orography. The atmosphere in the volume previously occupied by orography is derived from NAM initial analyses and uses a moist-adiabatic lapse rate at levels below the NAM model surface. Given the small upstream orographic volume removed, and the 6–9-h integration time prior to lake-effect precipitation, our results are likely insensitive to these prescribed initial conditions.

In the FLAT-NL and no-lake (NL) simulations, points over the GSL are converted from water to barren, sparsely vegetated land. Land surface characteristics, including soil moisture, soil temperature, albedo, and land surface temperature, are interpolated across the GSL area from adjacent land points.

3. Results

a. Observed evolution

On 27 October 2010 GSL-effect precipitation developed in the wake of a baroclinic trough that passed the Salt Lake City International Airport (KSLC) shortly after 0000 UTC. During the event (0600 UTC), a 500-hPa shortwave trough was located over northern Utah (Fig. 4a).

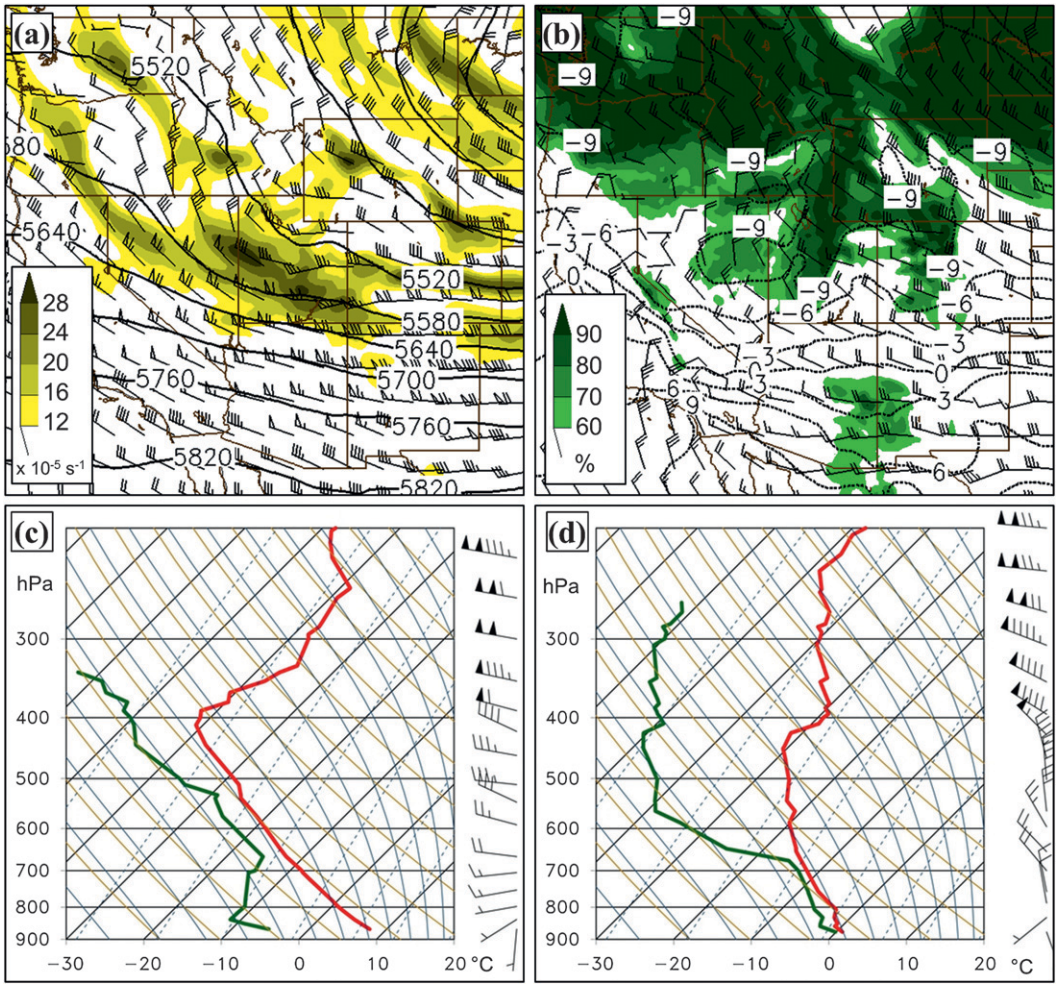

FIG. 4. Environmental conditions for 27 Oct 2010. (a) 500-hPa geopotential height (contours every 60 m), wind (full and half barb denote 5 and 2.5 m s^{-1}, respectively), and absolute vorticity ($\times 10^{-5}$ s^{-1}, scale at left) at 0600 UTC. (b) 700-hPa temperature (black contours every 3°C with negative contours dashed), 700-hPa winds [as in (a)], and 850–700-hPa mean relative humidity (%, shaded, scale at left) at 0600 UTC. (c) Salt Lake City skew T–log$p$ diagram with temperature, dewpoint, and wind [as in (a)] at 0000 UTC. (d) As in (c), but for 1200 UTC.

At 700-hPa, a cold pool extended southward from Canada into Nevada, Utah, and Wyoming, with northwest flow over the GSL (Fig. 4b). The mean 850–700-hPa relative humidity was above 70% over much of northern Utah and southern Idaho, indicating sufficient low-level moisture for the GSL effect (Alcott et al. 2012). The 0000 UTC radiosonde observation from KSLC (Fig. 4c), launched downstream of the GSL prior to the passage of the baroclinic trough, featured a deep, dry convective boundary layer. Temperatures dropped and lake-effect precipitation features began to develop in KMTX radar reflectivity imagery at ~0228 UTC. The 1200 UTC sounding from KSLC, launched late in the event, showed near-saturated, moist-adiabatic conditions from the surface through 670 hPa, with dry air above ~675 hPa (Fig. 4d). Light southerly and southwesterly winds were observed near the surface, whereas winds above 800 hPa were northerly and northwesterly. Based on satellite-derived skin temperature data collected prior to the event on 25 October, the median GSL water temperature was 13.3°C, which yields lake–700-hPa temperature differences of 21.8° and 25.0°C given the observed 700-hPa temperatures of –8.5° and −11.7°C at 0000 and 1200 UTC, respectively.

Figure 5 shows the KMTX 0.5° radar reflectivity and MesoWest surface winds at 0400, 0600, 0900, and 1100 UTC. At 0400 UTC, a wide band of radar echoes extended from the Promontory Mountains over the southeast shore of the GSL and into the Wasatch Mountains (Fig. 5a). Winds were 7.5–10 m s^{-1} and from the west-northwest over the Great Salt Lake Desert and along the western shore of the GSL, but light and

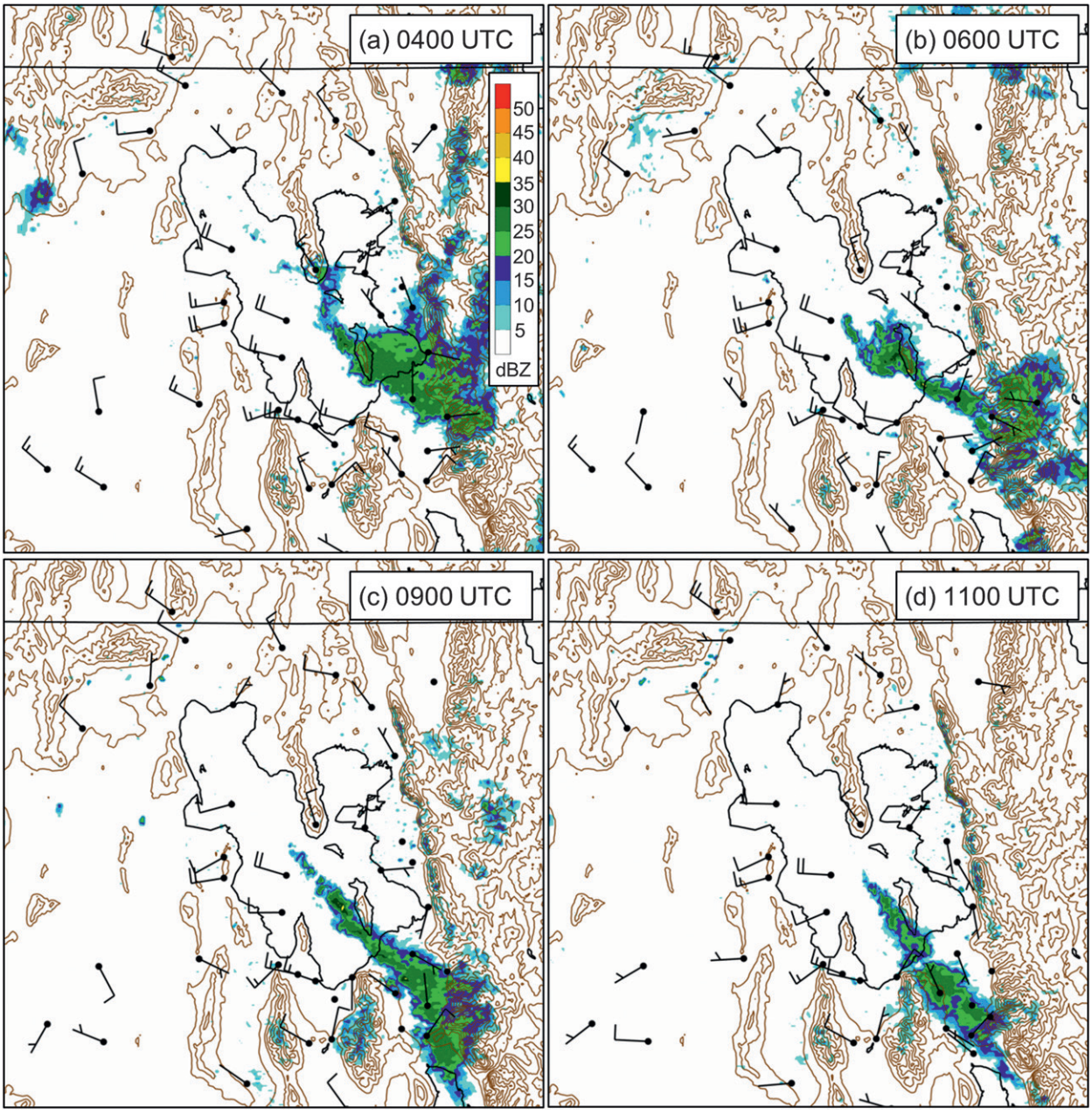

FIG. 5. Terrain (brown contours every 200 m), KMTX 0.5° radar reflectivity [dBZ, shaded, scale in (a)], and MesoWest winds (full and half barb denote 5 and 2.5 m s^{-1}, respectively) at (a) 0400, (b) 0600, (c) 0900, and (d) 1100 UTC 27 Oct 2010.

variable along the northern Wasatch Front and in the Salt Lake Valley. The band narrowed after 0400 UTC and occasionally produced radar echoes ≥35 dBZ (Figs. 5b,c). By 1100 UTC the band began moving westward through the Salt Lake Valley toward the Oquirrh Mountains (Fig. 5d). Precipitation diminished after 1200 UTC and by 1659 UTC radar echoes were no longer observed in association with the GSL (not shown). Based on this analysis, we define the start and end of the 27 October 2010 event as 0228 and 1659 UTC, respectively.

During the 27 October 2010 event, light rain that changed to light snow between 0253 and 0350 UTC produced 7 mm of SWE at KSLC, with visibilities reduced to 0.5 mi (800 m) near 0500 UTC (Fig. 6a). In the Wasatch Mountains southeast of the GSL, 30 cm of snow fell (based on the change in total snow depth) at the Alta-Collins snow study plot (CLN, see Fig. 1 for location), with a total of 23 mm of SWE (Fig. 6b). Radar-derived quantitative precipitation estimates based on a reflectivity–SWE (Z–S) relationship of $Z = 75S^2$

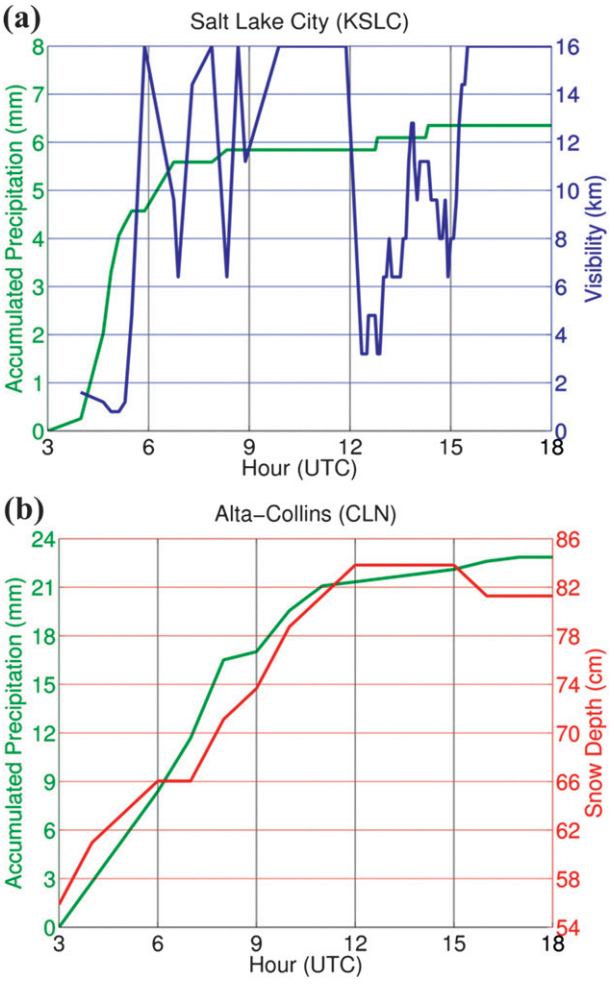

FIG. 6. Observations from the 27 Oct 2010 GSL-effect event. (a) KSLC accumulated precipitation (mm, green line) and visibility (km, red line). (b) CLN accumulated precipitation (mm SWE, green line) and total snow depth (cm, red line).

(Rasmussen et al. 2003) suggest that 6–10 mm of SWE fell across much of the Salt Lake Valley, consistent with the available gauge observations, with an embedded banded maximum >15 mm (Fig. 7). This methodology underestimates precipitation amounts in the Wasatch Mountains where gauge observations indicate that accumulations were greatest (15–23 mm), a result that might reflect partial beam blockage or poorly sampled near-surface orographic precipitation enhancement.

b. *Simulated evolution in CTL*

CTL produces a lake-effect band that is similar to the observed, with some differences in intensity and position after 0600 UTC. To facilitate comparison with the observed radar reflectivity (Fig. 5), Fig. 8 presents the WRF-simulated radar reflectivity at 2500 m MSL (roughly the height of the centroid of the KMTX 0.5° scan near the southeast shore of the GSL), which was calculated from the model hydrometeor mixing ratios assuming spherical particles of constant density with exponential size distributions. At approximately 0400 UTC, CTL produces precipitation over and downstream of a confluence zone that extends from near the southern end of the Promontory Mountains to the northern Salt Lake Valley (Fig. 8a). Model diagnostics (not shown) indicate that winds in this confluence zone are convergent, and hereafter we refer to it as a convergence zone. At 0600 UTC, the convergence zone extends along the entire long axis of the GSL, with northwesterly and westerly flow from west of the GSL meeting northerly flow along the western slopes of the Promontory Mountains and over the southeastern GSL (Fig. 8b). Winds are light and variable over the northern Wasatch Front and in the Salt Lake Valley. Precipitation extends downstream from the southeast portion of the convergence zone, broadening near and over the Wasatch Mountains. As observed, the simulated band peaks in intensity from around 0600 to 0700 UTC.

By 0900 UTC, the axis of the simulated precipitation band remains well organized but is ~(10–20) km southwest of observed (cf. Figs. 5c and 8c). This difference is perhaps due to a more northerly 10-m wind component than observed over western portions of the GSL. The simulated winds along the southwestern shore remain northwesterly throughout the event, whereas observed winds in this region were consistently from the west-southwest. Steenburgh and Onton (2001) encountered similar issues in simulations of the 7 December 1998 GSL-effect event. Although the position of the simulated band differs slightly from observed, the general structure and horizontal extent are well represented by CTL through 1100 UTC, when the simulated band begins to dissipate (Fig. 8d). Simulated precipitation ends by 1300 UTC, approximately 4 h prior to the observed end of the event, although the observed precipitation was very light after 1300 UTC.

The simulated 0230–1700 UTC SWE totals of 12–20 mm in Wasatch Mountains are in good agreement with gauge observations (cf. Figs. 7 and 9a; e.g., 23 mm at CLN and 15–20 mm at nearby sites). Simulated precipitation over the Salt Lake Valley is also in good agreement, although totals in CTL are 2–8 mm more than suggested by radar-derived estimates and the observed total at KSLC, and the banded precipitation maximum in CTL is 5–10 km southeast of the observed radar-derived maximum. Accumulations in the elongated precipitation maximum south of Antelope Island are also greater in CTL (up to 26.8 mm) than the radar estimate (up to 18.7 mm). Over the lake-effect region (the domain

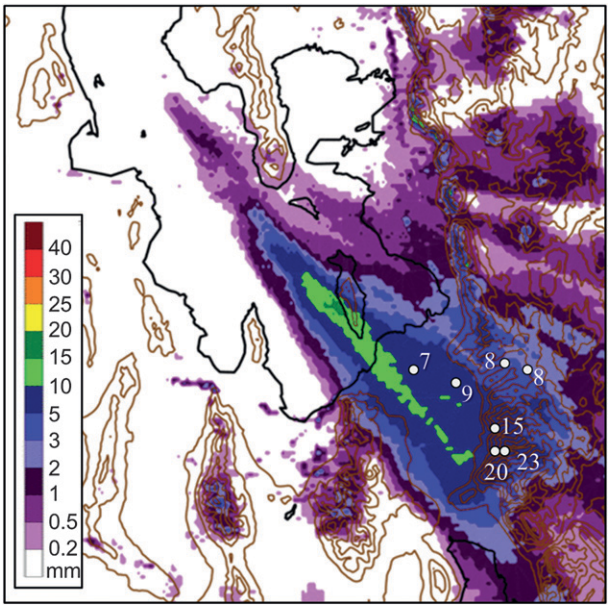

FIG. 7. Terrain (brown contours every 200 m), radar-estimated precipitation (mm, shaded, scale at left), and gauge-measured precipitation (mm, annotated) at available stations from 0230 to 1700 UTC 27 Oct 2010.

shown in Figs. 9a–f), the mean precipitation in CTL is 1.10 mm, with a maximum of 26.8 mm, and an area of 731 km^2 receiving more than 10 mm (Table 1).

c. *Sensitivity to orography*

Sensitivity studies show that both GSL and the orography downstream are crucial to the development of a significant precipitation event. Here we present a brief summary of the sensitivity study results, followed by a more detailed examination of the relevant physical processes in the next section. Table 1 summarizes the total precipitation produced by each simulation from 0230 to 1700 UTC within the lake-effect region displayed in Fig. 9.

In FLAT-NL, no precipitation develops from 0230 to 1700 UTC (Fig. 9b; Table 1). In FLAT, the mean simulated precipitation is only 0.05 mm, 94% less than CTL, with a maximum of only 3.2 mm (Fig. 9c; Table 1). The simulated precipitation in FLAT only briefly organizes into a band, which shifts southwestward and fluctuates in intensity, leaving three weak, elongated accumulated precipitation maxima. This dramatic decrease in precipitation with the removal of orography contrasts with the findings of Onton and Steenburgh (2001; cf. their Figs. 17a and 21) for the 7 December 1998 event. Their "FLAT" simulation produced only 7% less domain-averaged precipitation than their control, with the only major difference in precipitation occurring where their lake-effect band intersected the Oquirrh Mountains.

Including only the Wasatch Mountains (WAS) yields a mean precipitation of 0.80 mm (27% less than CTL), a maximum of 21.6 mm, and a 214 km^2 area with more than 10 mm (Fig. 9d; Table 1). Adding the remaining downstream terrain (DT) yields a mean precipitation of 1.77 mm (61% greater than CTL), a maximum of 41.9 mm, and a 1703 km^2 area with more than 10 mm (Fig. 9e; Table 1). The lack of upstream terrain in DT allows cold, moist air from the Snake River Plain to move directly over the GSL without orographic modification. This leads to a more intense precipitation band that dissipates later [after 1500 UTC (not shown)] and produces the greatest increase in precipitation relative to CTL. Removing the GSL in NL reduces the mean precipitation to 0.11 mm, 90% less than CTL, and the maximum to 2.5 mm, with precipitation almost entirely confined to high elevations (Fig. 9f; Table 1). These results illustrate that synergistic interactions between lake and orographic processes are crucial for precipitation during the 27 October 2010 event, as simulations without terrain (e.g., FLAT) or without the GSL (e.g., NL) produce very little precipitation. It is only when both the GSL and the downstream terrain are included that the WRF produces substantial precipitation.

d. *Upstream orographic influences*

The Jarbidge–Caribou Highlands north and northwest (upstream) of the GSL (see Fig. 1) have a significant effect on the low-level thermal and moisture characteristics of the air mass that moves over the GSL. In CTL, the relative humidity at the lowest half-sigma level is considerably lower downstream of the Jarbidge–Caribou Highlands compared to upstream over the southern Snake River Plain (Fig. 10a). The drying extends from the surface through the midtroposphere, as evidenced by a cross section from the Snake River Plain to the north arm of the GSL (Fig. 10b). The low-level potential temperature is also about 4 K greater downstream of the Jarbidge–Caribou Highlands. This leeward drying and warming resembles that observed during the Alpine foehn and similar downslope events in other regions and can be produced by two mechanisms (Richner and Hächler 2012). The first is latent heating and drying during wet-adiabatic ascent and orographic precipitation over a mountain barrier, which yields a net increase in potential temperature and decrease in specific humidity that is sometimes referred to as airmass transformation (e.g., Smith et al. 2003, 2005). The second is leeward dry-adiabatic descent, which occurs when the upstream air mass is stable and blocked at low levels, and upper-level air descends in the lee of the barrier, leading to dry adiabatic descent and relative drying of the higher-θ air originating aloft. Some additional

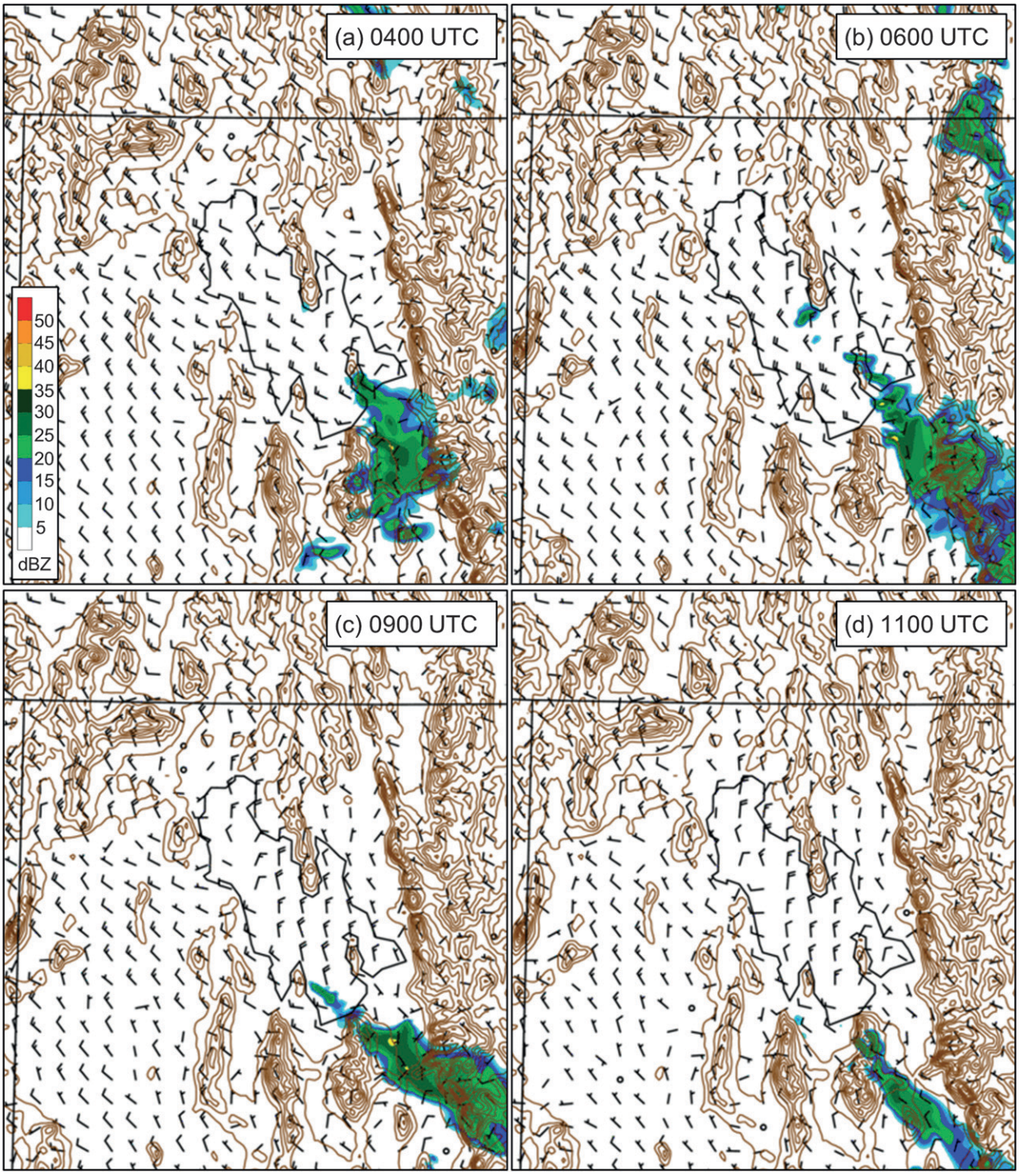

FIG. 8. CTL terrain (brown contours every 200 m), 10-m wind (full and half barb denote 5 and 2.5 m s^{-1}, respectively), and simulated 2500-m MSL radar reflectivity [dBZ, shaded, scale in (a)] at (a) 0400, (b) 0600, (c) 0900, and (d) 1100 UTC 27 Oct 2010.

diabatic airmass modification is possible through turbulent motions in orographic moist convection and/or mountain waves.

In CTL, less than 0.2 mm of SWE fell over the upstream orography, suggesting that airmass transformation was not the dominant contributor to the leeward drying and warming. Instead, the dominant contributor was the dry-adiabatic warming and drying of the flow aloft as it descended into the GSL basin. For example, at 0700 UTC, the low-level flow in CTL north of the Jarbidge–Caribou

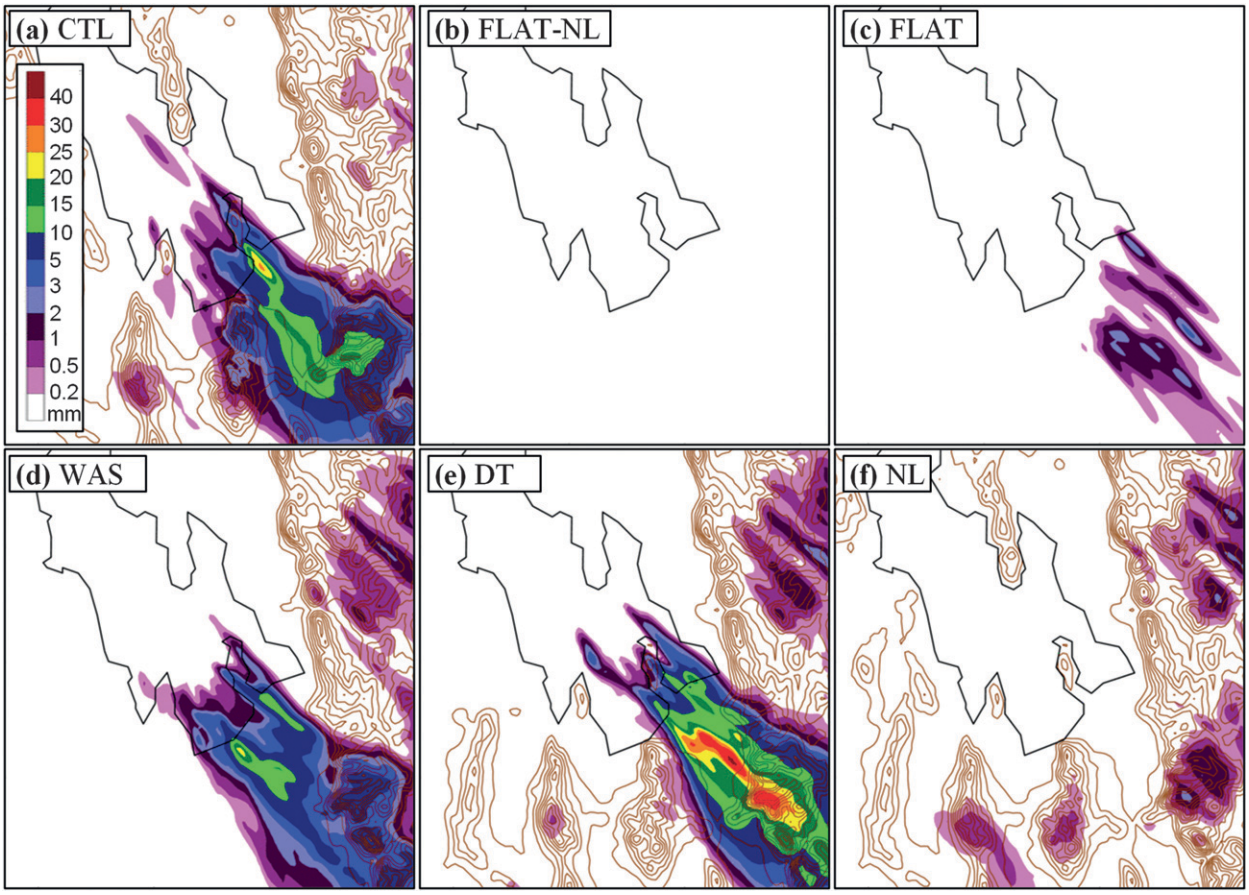

FIG. 9. Terrain (brown contours every 200 m) and simulated precipitation [mm, shaded, scale in (a)] for (a) CTL, (b) FLAT-NL, (c) FLAT, (d) WAS, (e) DT, and (f) NL from 0230–1700 UTC 27 Oct 2010. Lake outlines in (b) and (f) are shown for reference only.

Highlands was channeled along the Snake River Plain (Fig. 11a). Steenburgh and Blazek (2001) observed a similar channeling effect in this region behind a cold front on 3 December 1998. In contrast, when the Jarbidge–Caribou Highlands and other nearby terrain features are removed in DT, the northwesterly flow penetrates unimpeded over the GSL (Fig. 11b). Many of the trajectories that terminate over the north arm of the GSL in CTL begin at ~2000 m MSL (~700 m AGL) over the Snake River Plain (Fig. 12; e.g., orange and red trajectories). These trajectories reach an altitude of ~2500 m MSL over the Jarbidge–Caribou Highlands and then descend to ~1300 m MSL over the GSL, which corresponds to a net descent of ~700 m and an adiabatic temperature increase of ~7 K. Weak maxima in potential temperature and minima in specific humidity occur along these trajectories where they move through orographic clouds and the relative humidity reaches 100%. However, the largest net decrease in specific humidity along these trajectories during this period (0830–1030 UTC) is only 0.6 g kg^{-1} (see red trajectory). If this decrease is entirely the result of condensation, it accounts for a net diabatic warming of only ~2 K, much smaller than the warming due to dry adiabatic descent (the potential temperature

TABLE 1. Simulated precipitation statistics from 0230 to 1700 UTC 27 Oct 2010 for the domain shown in Fig. 9.

Event	Expt	Description	Mean precipitation (mm)	Change from CTL (%)	Max precipitation (mm)	Area of ≥10 mm precipitation (km^2)
27 Oct 2010	FLAT-NL	Flat, no lake	0.00	−100	0.0	0
27 Oct 2010	FLAT	Flat domain	0.07	−94	3.2	0
27 Oct 2010	WAS	Wasatch only	0.80	−27	21.6	214
27 Oct 2010	DT	Downstream only	1.77	+61	41.9	1703
27 Oct 2010	CTL	Real orography	1.10	—	26.8	731
27 Oct 2010	NL	No lake	0.11	−90	2.5	0

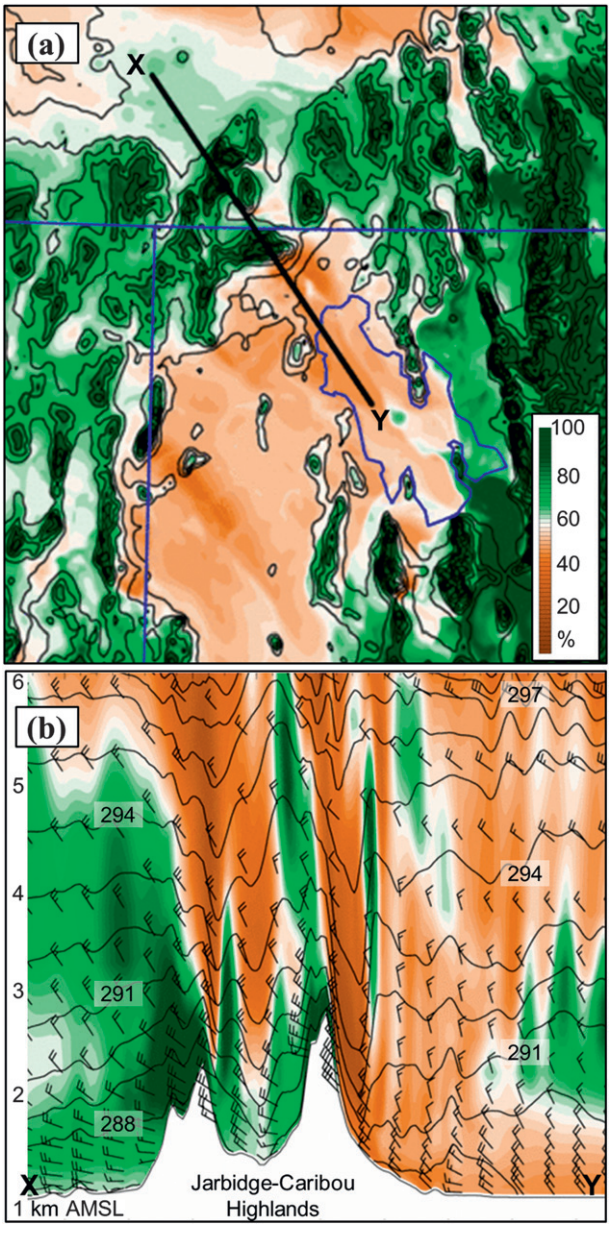

FIG. 10. (a) CTL terrain (black contours every 200 m) and lowest half-sigma-level relative humidity (%, shaded, scale at right) at 0700 UTC 27 Oct 2010. (b) CTL relative humidity [%, shaded, scale in (a)], potential temperature (contours every 1 K) and wind (full and half barb denote 5 and 2.5 m s^{-1}, respectively) averaged over 5 km on either side of cross section *X*–*Y* in (a) at 0700 UTC 27 Oct 2010.

change along this trajectory from 0830 to 1030 UTC was only 1 K). Therefore, we conclude that dry adiabatic descent dominates the warming and drying produced in the foehnlike flow over the Jarbidge–Caribou Highlands, although it is possible that airmass transformation could play a more prominent role in other events.

Although a small contributor to the total mass flux across the Jarbidge–Caribou Highlands, cold air from the Snake River Plain does penetrate into the GSL basin through some low-elevation gaps. For example, the light green trajectory in Fig. 12 passes through Moburg Canyon, the lowest gap in the Jarbidge–Caribou Highlands northwest of the GSL. This trajectory originates over the Snake River Plain at ~1500 m MSL, reaches ~2000 m MSL as it ascends into upper Moburg Canyon, and then descends into the GSL basin, resulting in a net vertical displacement of <200 m. Once entering the GSL basin, trajectories moving through Moburg Canyon are quickly "scrambled" with others that originate at higher elevations and have experienced greater net subsidence (e.g., the green trajectory in Fig. 12). Smith et al. (2003) describe a similar scrambling of trajectories downstream of the Alps.

The Jarbidge–Caribou Highlands also affect the flow kinematics over the north arm of the GSL. At 0700 UTC, a pronounced wake with an anticyclonic eddy and complete flow reversal exists downstream of the Raft River Range, which rises to the west of Moburg Canyon and is one of the higher barriers in the Jarbidge–Caribou Highlands (Fig. 11a). Observations of light and variable winds downstream of the Raft River Range from 0600 to 1200 UTC provide evidence for the existence of this wake (Figs. 5b–d). A smaller wake also forms in the lee of the foothills south of the Raft River Mountains (Fig. 11a). These obstacle effects, combined with blocking windward of the Promontory Point, generate convergent flow over the north arm of the GSL.

This convergence appears to influence the structure and evolution of the lake-effect band. For example, the lake-effect band in CTL is slightly narrower and longer than in DT and forms in the middle of the lake rather than on the southeast shore, despite warming and drying of the upstream flow during flow over the Jarbidge–Caribou Highlands in CTL (cf. Figs. 11a,b). Although the potential sensitivity of modeled convection to small differences in the two simulations precludes a definitive assessment, other studies suggest that upstream terrain can affect precipitation dynamics. For example, topographic convergence contributes to precipitation downstream of the Olympic Mountains and over the Snake River Plain (Mass 1981; Mass and Dempsey 1985; Chien and Mass 1997; Andretta and Hazen 1998). In addition, Tripoli (2005) suggests that variations in the upstream shore geometry can help generate streamwise vorticity and contribute to the development of roll convection during lake-effect storms over the Great Lakes.

The removal of upstream terrain in DT yields a near-uniform northwest flow pattern over the north arm of the GSL at 0700 UTC (Fig. 11b). Although the convergence

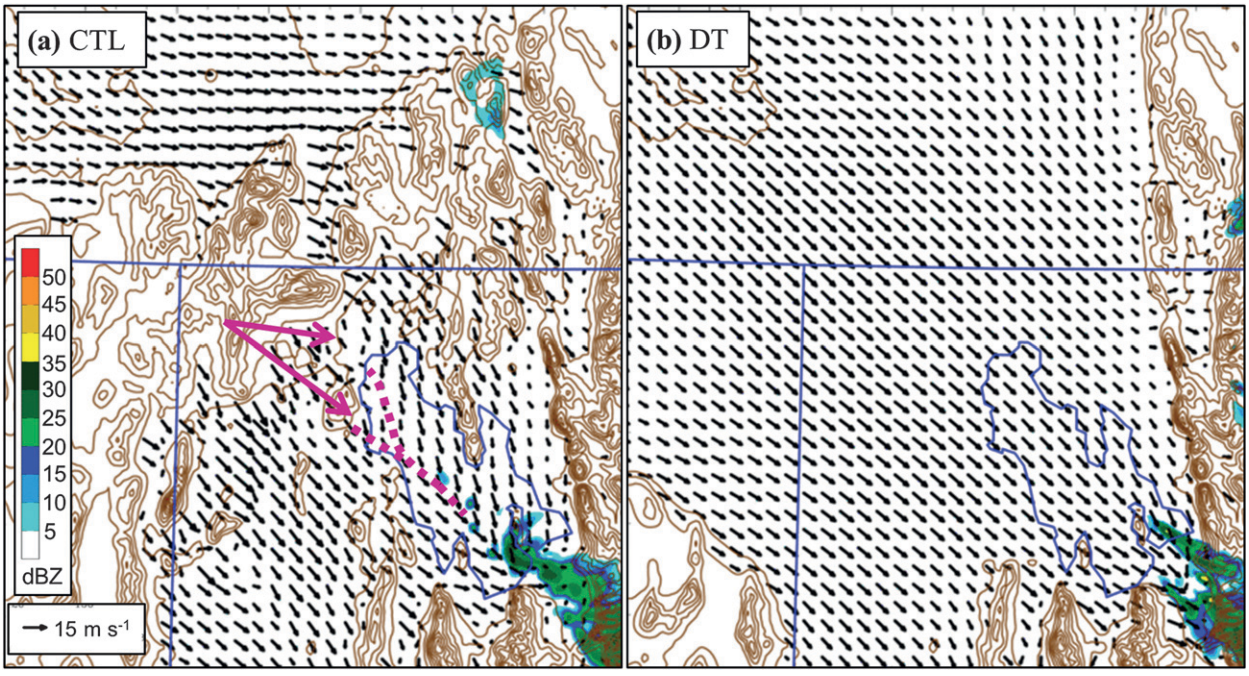

FIG. 11. Terrain (brown contours every 200 m), 1600-m wind vectors (scale near bottom left), and simulated 2500-m radar reflectivity [dBZ, shaded, scale in (a)] at 0700 UTC 27 Oct 2010 for (a) CTL and (b) DT. Purple arrows and dashed lines indicate wakes and convergence zones, respectively.

generated by the upstream orography is lost, the movement of cooler, moister air directly from the Snake River Plain over the GSL yields more precipitation in DT than in CTL (cf. Figs. 9a,e). This finding is consistent with Kristovich and Laird (1998), who found lake-effect intensity is sensitive to upstream moisture conditions.

e. Downstream orographic influences

Past work on the orographic modification of lake effect has primarily dealt with enhancement through microphysical processes and increased vertical motions during upslope flow (e.g., Hjelmfelt 1992; Saito et al. 1996; Kusunoki et al. 2004). The situation in the 27 Oct 2010 GSL-effect event calls for the consideration of other processes, including blocking and flow channeling into the orographic concavity formed by the Wasatch and Oquirrh Mountains. CTL produces 16 times more mean precipitation (1.10 mm) than FLAT (0.07 mm), suggesting a strong synergistic interaction between lake and mountain processes (cf. Figs. 9a,c; Table 1).

During the event (e.g., 0700 UTC), a convergence zone develops over southeast portions of the GSL that is much stronger in simulations with terrain than those without (Fig. 13). In CTL, WAS, and DT, the convergence zone position varies by 10–20 km, but in all three simulations it lies between moderate northwest winds over the western half of the GSL and northerly or weak flow over the eastern GSL and northern Wasatch Front (Figs. 13a,d,e). This convergence zone serves as the locus for precipitation initiation in CTL, WAS, and DT.

The weak northerly low-level flow over the eastern GSL and northern Wasatch Front is not an inherent attribute of the background flow, as evidenced by the uniform, northwesterly flow in FLAT-NL at 0700 UTC (Fig. 13b). The addition of the GSL in FLAT results in only weak thermally driven convergence and light precipitation far downstream of the GSL (Fig. 13c). However, when the Wasatch Mountains are added in WAS, the low-level flow over the eastern GSL and northern Wasatch Front becomes northerly or weak, enhancing the convergence and resulting in precipitation over and southeast of the GSL (Fig. 13d). The addition of the Oquirrh Mountains in DT yields easterly deflection of the flow over the southwest GSL into the Salt Lake Valley, further enhancing the low-level convergence and precipitation (cf. Figs. 13d,e). In fact, the mean precipitation in DT (1.77 mm) is more than double that of WAS (0.80 mm) and exceeds that of CTL (1.10 mm) owing to the lack of airmass warming and drying due to upstream orography.

The funneling of the flow and precipitation enhancement in the Salt Lake Valley resembles that which occurs during flow into terrain concavities. For example, concavities in the Alps are associated with climatological precipitation maxima (Frei and Schär 1998) and produce

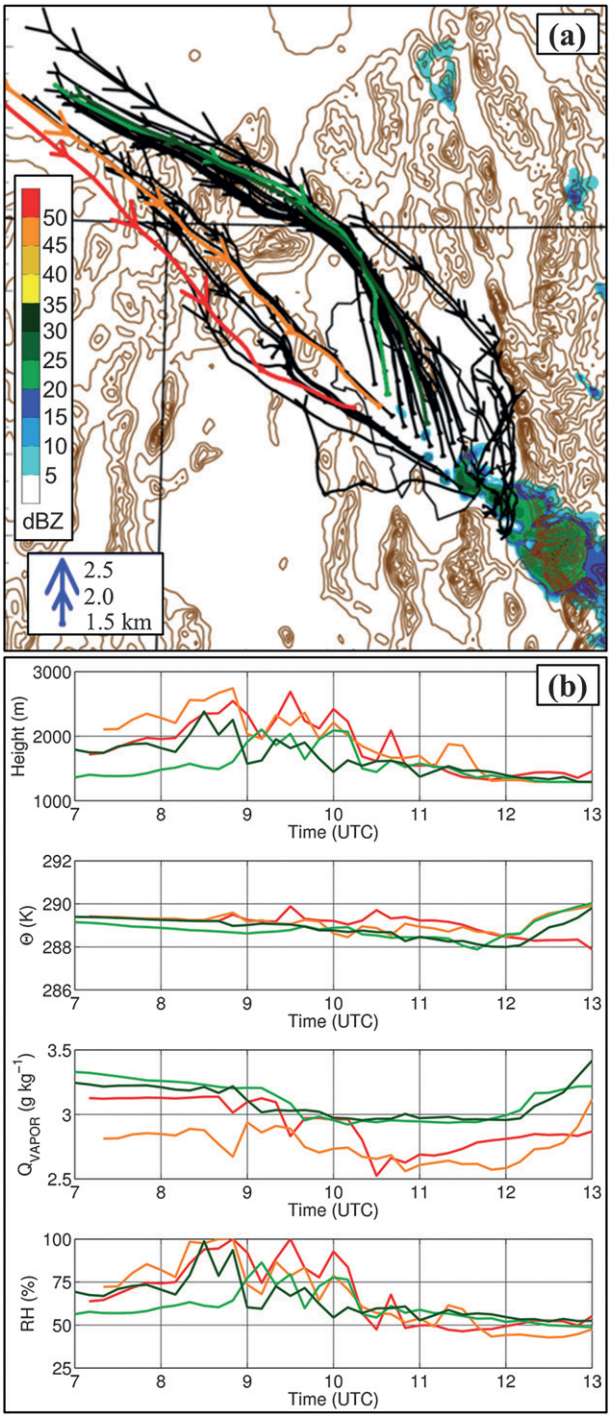

FIG. 12. (a) CTL trajectory paths beginning at 0100 UTC and ending at 0700 UTC 27 Oct 2010 and simulated 2500-m radar reflectivity (dBZ, shaded, scale at left) at 0700 UTC 27 Oct 2010. Trajectory altitude (m MSL) indicated by arrow size, with scale at lower left. (b) Altitude (m MSL), potential temperature, water vapor mixing ratio, and relative humidity along selected trajectory paths in (a).

low-level convergence and precipitation enhancement during some precipitation events (Schneidereit and Schär 2000; Gheusi and Davies 2004). In stratified moist flow, idealized numerical modeling studies produce enhanced convergence and precipitation within terrain concavities compared to linear or convex ridges (Jiang 2006; Watson and Lane 2012).

The Wasatch and Oquirrh Mountains act collectively as a discontinuous concave ridge during the 27 October 2010 event (the ridge is discontinuous because of the existence of the intermediate Salt lake Valley). Mountain ranges farther to the west (i.e., the Stansbury and Cedar Mountains) broaden the horizontal scale of the discontinuous concavity. In idealized simulations, Watson and Lane (2012) show that outer portions of a concave ridge deflect flow inward to yield flow deceleration, convergence, and enhanced upward motions. A comparison of the low-level flows in WAS and DT supports this conceptual model. In DT, northwest flow approaching the Oquirrh Mountains is deflected eastward into the Salt Lake Valley, producing an area of confluence (Fig. 13e). This confluence zone is shifted eastward from WAS (i.e., Fig. 13d), is convergent based on model diagnostics (not shown), and is collocated with the lake-effect precipitation. Although the coverage and magnitude of the simulated reflectivity is similar in WAS and DT at 0700 UTC, the mean event precipitation in DT is more than twice as large as in WAS.

Horizontal variations in static stability may further contribute to convergence near the southeast shore of the GSL. In CTL, the atmosphere within the lake-effect band is saturated or nearly saturated and moist neutral to ~525 hPa (Fig. 14a). However, the air mass impinging on the northern Wasatch Mountains is largely unmodified by the GSL, absolutely stable near the ground, and weakly stable for unsaturated parcel displacements from ~850 hPa to crest level [~700 hPa (Figs. 14b,c)]. Similarly, the flow impinging on the Oquirrh Mountains crosses only the southwest corner of the GSL and is also sufficiently stable to be deflected into the Salt Lake Valley (not shown). The end result is a funneling effect near the Salt Lake Valley due to blocking and deflection of statically stable flow by both the Northern Wasatch and Oquirrh Mountains.

It is likely that reinforcement of the lake-driven circulation by orographic blocking does not fully explain the intensity of the convergence and enhancement of precipitation in CTL and DT since latent heating from condensation and fusion contribute to a more vigorous cross-band circulation (e.g., Lavoie 1972; Hjelmfelt and Braham 1983; Hjelmfelt 1990; Onton and Steenburgh 2001). Passarelli and Braham (1981) refer to this as a "self-maintaining system." Thus, the event is ultimately

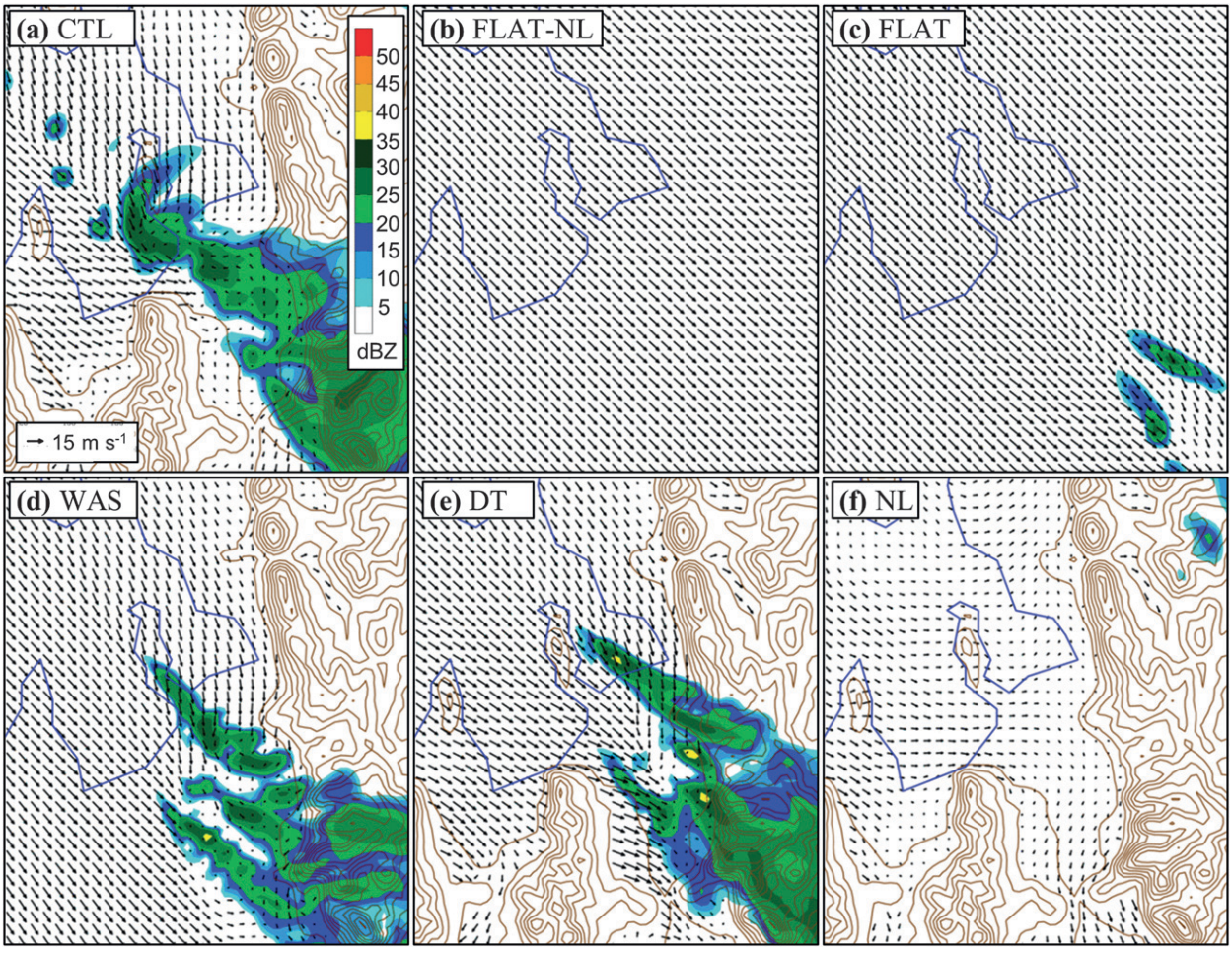

FIG. 13. Terrain (brown contours every 200 m), wind vectors at 1600 m [scale at lower left in (a)] and simulated 2500-m radar reflectivity [dBZ, shaded, scale in (a)] at 0700 UTC 27 Oct 2010 for (a) CTL, (b) FLAT-NL, (c) FLAT, (d) WAS, (e) DT, and (f) NL. Lake outlines in (b) and (f) are shown for reference only.

generated by nonlinear interactions between lake, orographic, and moist-diabatic processes.

Thermally driven flows associated with orography do not appear to play a significant role in the 27 October 2010 event. In a quiescent weather pattern when thermally driven flows dominate, katabatic slope, valley, and gap flows have been observed around the GSL (Stewart et al. 2002; Chrust et al. 2013) and could potentially affect GSL-effect events by contributing to offshore flow and overlake convergence. We examined the potential role of katabatic flows associated with the Wasatch Mountains by comparing observed surface winds near the GSL with those further to the east at the base of the mountains. A weak offshore flow component is observed along the eastern shore of the GSL at station QSY (see Fig. 1), with east winds of 3–6 m s^{-1} after 0600 UTC (Fig. 15a), but winds at station PWR (see Fig. 1) in Weber Canyon remain out of the west at 3–8 m s^{-1} throughout the event (Fig. 15b), indicating that nocturnal downslope and gap flows did not contribute to overlake convergence. The observed up-canyons flows are likely forced by a northeast–southwest-oriented mean sea level pressure gradient across the domain (not shown).

Observed precipitation within the 27 October 2010-lake band increases considerably with elevation, reaching a maximum of 23 mm of SWE at CLN in the Wasatch Mountains southeast of the GSL. These data reflect a precipitation–altitude relationship that has been frequently observed downstream of the GSL and other bodies of water (e.g., Hill 1971; Reinking et al. 1993; Saito et al. 1996; Steenburgh and Onton 2001; Onton and Steenburgh 2001; Steenburgh 2003; Yeager et al. 2013). Potential contributors to the increase in precipitation with elevation include the following: 1) increased vertical motions forced by steep terrain, 2) subcloud evaporation and/or sublimation over adjacent lowland

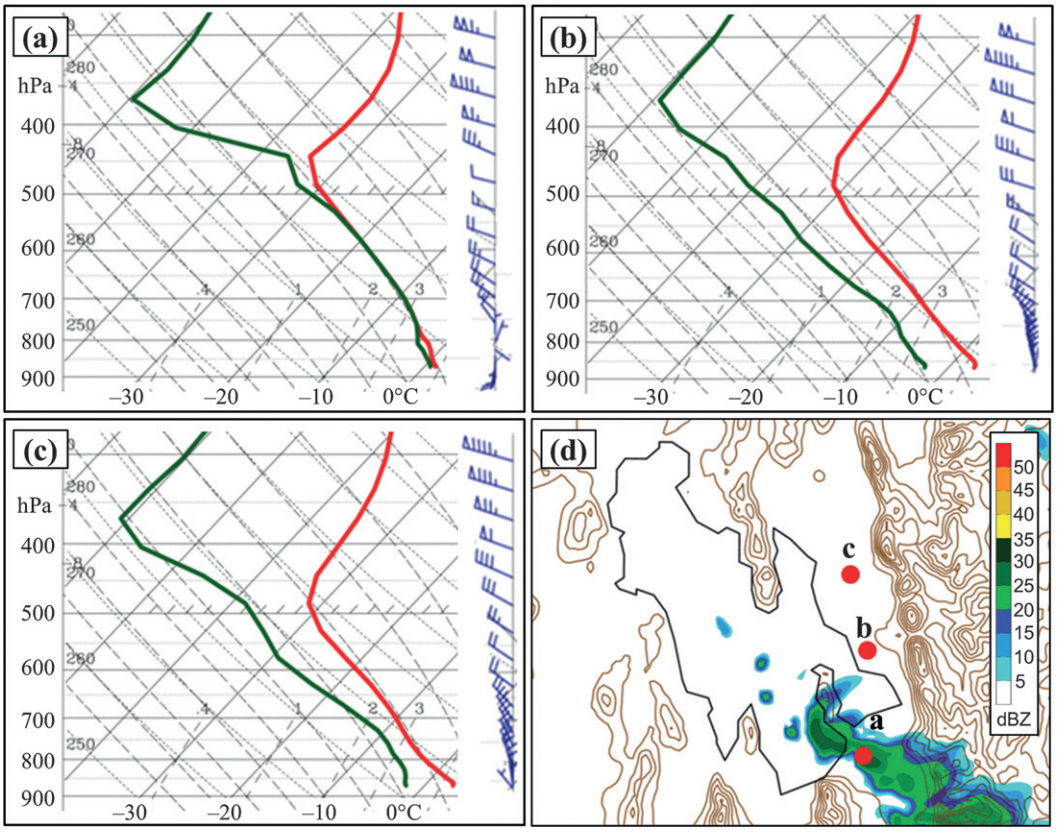

FIG. 14. (a)–(c) CTL skew T–log$p$ profiles with temperature, dewpoint, and wind (full and half barb denote 5 and 2.5 m s^{-1}, respectively) at 0700 UTC 27 Oct 2010. Indicated on the map in (d) are the locations of the profiles. (d) CTL terrain (brown contours every 200 m) and 2500-m simulated radar reflectivity (dBZ, shaded, scale at right).

areas, 3) advection of slow-falling hydrometeors into downstream terrain, and 4) increased precipitation efficiency due to higher ice-nucleation rates when parcels are lifted to colder temperatures (e.g., Saito et al. 1996).

The largest contributor to orographic enhancement in CTL appears to be hydrometeor advection. Along a cross section from Antelope Island to the east side of the Wasatch Mountains, the strongest vertical motions in CTL occur over the GSL rather than the high terrain, and subcloud sublimation over the Salt Lake Valley is likely small because the relative humidity is greater than 90% from the surface to 4 km (Fig. 16a). In addition, the depth of the storm decreases downstream along the cross section, and thus the Wasatch Mountains do not produce a region where temperatures are colder and ice nucleation is more likely than over the valley (e.g., Saito et al. 1996). However, the largest snow mixing ratios are over the GSL and most 1-h hydrometeor trajectories from this area lead directly to high elevations of the Wasatch Mountains (Fig. 16b). This calculation is reasonable given an approximate 30-km horizontal transport in 1 h at an elevation of 5 km, where observed and modeled winds were ~10 m s^{-1} (~36 km h^{-1}). Therefore, although the majority of hydrometeor growth occurs over the GSL, a large fraction of the hydrometeor mass is carried downstream into the Wasatch Mountains. These conclusions are subject to the ability of WRF to accurately simulate both convective motions and parameterized hydrometeor growth. Nonetheless, CTL presents a realistic scenario in which hydrometeor transport and fallout play a prominent role in the distribution of precipitation and the apparent enhancement of precipitation over the Wasatch Mountains during the 27 October 2010 event.

4. Summary

Observational analyses and numerical simulations show that upstream and downstream orography contributes significantly to the GSL-effect event of 27 October 2010, as summarized in Fig. 17. Upstream orographic effects include a foehnlike flow over the Jarbidge–Caribou Highlands, which warms and dries the upstream air mass impinging on the Great Salt Lake. Although this reduces event intensity, orographically forced convergence

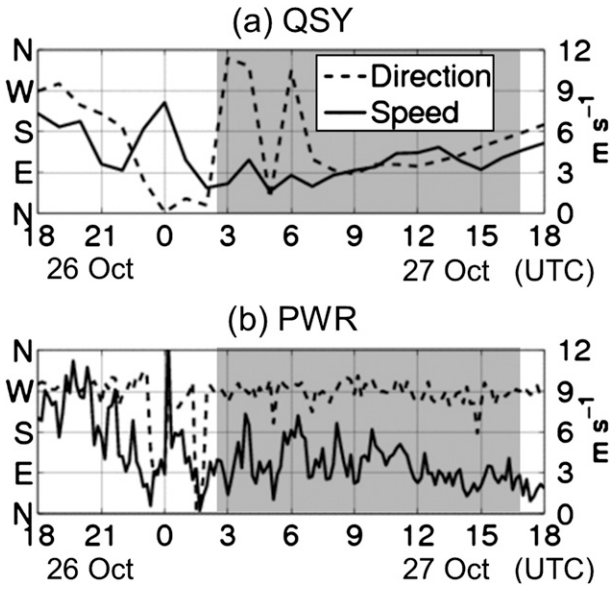

FIG. 15. Observed wind speed and direction at stations (a) QSY and (b) PWR (see Fig. 1 for locations). Gray-shaded area indicates the time range of the 27 Oct 2010 event.

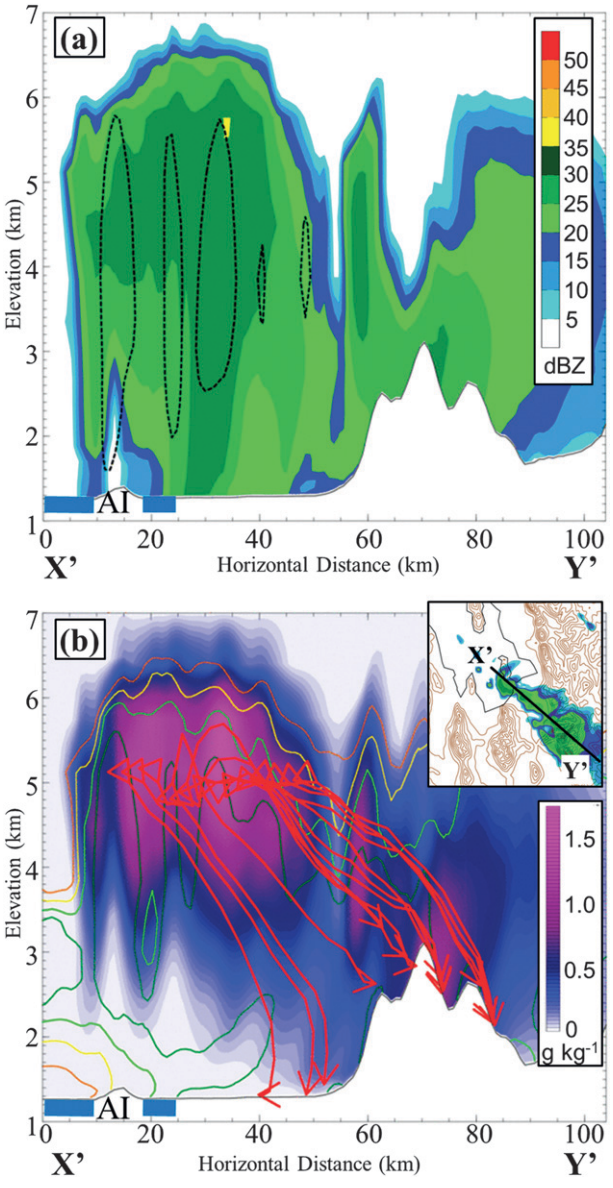

FIG. 16. (a) CTL 2500-m simulated radar reflectivity (dBZ, shaded, scale at right) and upward vertical velocity (dashed contour indicates 1 m s^{-1}) averaged over 5 km either side of cross section along line X'–Y' in top right inset. (b) CTL snow mixing ratio (g kg^{-1}, shaded, scale at right), relative humidity (brown, yellow, light green, dark green contours indicate 60%, 70%, 80%, and 90%, respectively), and 0700–0800 UTC hydrometeor trajectories (red lines). Lake indicated by thick blue line and Antelope Island by AI.

generated by flow around high orographic features and blocking by the Promontory Mountains extends downstream over the north arm of the GSL and affects the structure and evolution of the lake-effect precipitation band. Sensitivity studies indicate that the effects of the foehnlike flow offset any potential enhancement produced by the orographically forced convergence during the event. It is conceivable, however, that the importance of each of these effects varies from case to case depending on the thermodynamic and kinematic structure of the upstream flow.

Downstream orographic effects include the funneling of flow by the Wasatch and Oquirrh Mountains into the Salt Lake Valley, which reinforces the thermally driven convergence produced by the GSL. This funneling is similar to that produced by concave ridges (Schneidereit and Schär 2000; Gheusi and Davies 2004; Jiang 2006; Watson and Lane 2012) and strongly enhances the precipitation downstream of the GSL. Latent heating from condensation and fusion likely serves as an additional nonlinear feedback mechanism for enhancing the cross-band circulation and precipitation during the event.

Compared to the control (CTL) simulation that includes the GSL and surrounding (upstream and downstream) orography, simulations without the GSL (NL) or the surrounding terrain (FLAT) produce 90% and 94% less precipitation, respectively. Thus, our results demonstrate a situation where the GSL and the surrounding orography act synergistically to strongly enhance precipitation. Alcott (2012) showed that a very similar synergistic interaction occurred during the GSL-effect event of 5 November 2011. In contrast, the 7 December 1998 GSL-effect event examined by Steenburgh and Onton (2001) and Onton and Steenburgh (2001) was lake dominated, with moisture fluxes and thermally driven flows generated by the GSL producing a lake-effect precipitation band in much the same manner as

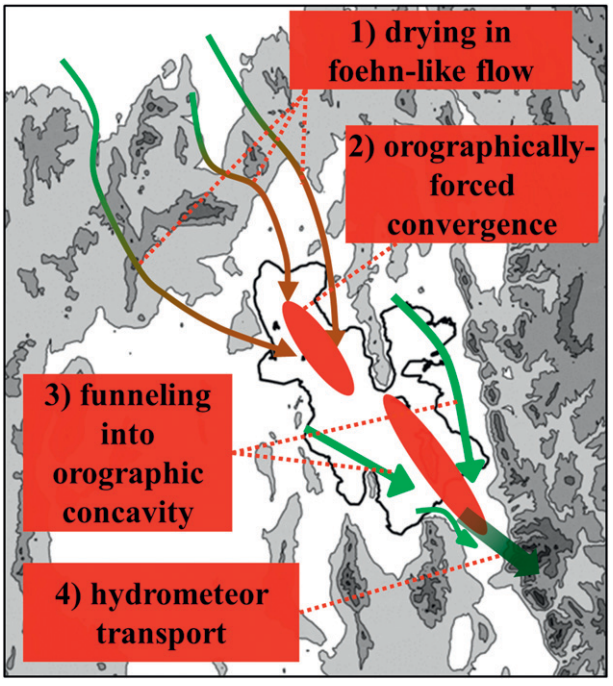

FIG. 17. Summary of the primary orographic influences on the 27 Oct 2010 GSL-effect event.

occurs over Lakes Michigan and Ontario, as well as over the English Channel and Irish Sea (e.g., Peace and Sykes 1966; Passarelli and Braham 1981; Braham 1983; Hjelmfelt 1990; Niziol et al. 1995; Norris et al. 2013). As a result, Onton and Steenburgh (2001) found that the domain-average precipitation decreased only 7% in the absence of orography (see their Table 1).

We propose that these events represent different points on the lake-orographic forcing spectrum. During lake-dominated events (e.g., 7 December 1998), surface fluxes and boundary layer circulations induced by the GSL dominate precipitation dynamics, and orographic processes play a minimal role in the storm initiation and morphology, although precipitation enhancement can occur where the lake-effect band intersects the orography. In the events of 27 October 2010 and 5 November 2011, lake and orographic processes act synergistically to generate or strongly enhance precipitation.

The lake–mountain environment of the GSL basin, especially the height and complexity of the orography, is unusual for the lake-effect regions of North America, but the results of this study retain broader applicability to the smaller terrain of the Laurentian Great Lakes, Lake Champlain, and the Finger Lakes. For example, Laird et al. (2009) suggest that orographic flow channeling enhances overlake convergence and precipitation during lake-effect events over Lake Champlain. The superposition of lake- and orographically generated convergence zones may have a particularly large impact on lake effect associated with small water bodies where fetch is limited. In a larger context, lake-effect storms associated with the Sea of Japan and Black Sea occur near terrain similar in scale to that of the GSL basin. Further research is needed to better elucidate and understand the lake-orographic forcing spectrum in these and other regions.

Acknowledgments. We thank Meteorologist-in-Charge Larry Dunn and Science Operations Officer Randy Graham of the National Weather Service Forecast Office in Salt Lake City for their guidance and two anonymous reviewers for comments and suggestions that helped strengthen the manuscript. This work was conducted in pursuit of a Doctor of Philosophy degree and we thank committee members John Horel, Steven Krueger, and Neil Laird. We gratefully acknowledge the provision of datasets, software, and/or computer time and services provided by NCDC, NCEP, NCAR, Unidata, the University of Wyoming, and the University of Utah Center for High Performance Computing. This article is based in part on research supported by Grant AGS-0938611 from the National Science Foundation and a series of grants provided by the NOAA/National Weather Service CSTAR program. Any opinions, findings, and conclusions or recommendations expressed herein are those of the authors and do not necessarily reflect those of the National Science Foundation or the NOAA/National Weather Service.

REFERENCES

Alcott, T. I., 2012: Environmental and orographic influences on Great Salt Lake–effect precipitation. Ph.D. dissertation, University of Utah, 130 pp.

——, W. J. Steenburgh, and N. F. Laird, 2012: Great Salt Lake–effect precipitation: Observed frequency, characteristics, and associated environmental factors. *Wea. Forecasting,* **27,** 954–971.

Andretta, T. A., and D. S. Hazen, 1998: Doppler radar analysis of a Snake River Plain convergence event. *Wea. Forecasting,* **13,** 482–491.

Braham, R. R., 1983: The Midwest snow storm of 8–11 December 1977. *Mon. Wea. Rev.,* **111,** 253–272.

Carpenter, D. M., 1993: The lake effect of the Great Salt Lake: Overview and forecast problems. *Wea. Forecasting,* **8,** 181–193.

Chen, F., and J. Dudhia, 2001: Coupling an advanced land surface–hydrology model with the Penn State–NCAR MM5 modeling system. Part I: Model implementation and sensitivity. *Mon. Wea. Rev.,* **129,** 569–585.

Chien, F.-C., and C. Mass, 1997: Interaction of a warm-season frontal system with the coastal mountains of the western United States. Part II: Evolution of a Puget Sound convergence zone. *Mon. Wea. Rev.,* **125,** 1730–1752.

Chrust, M. F., C. D. Whiteman, and S. W. Hoch, 2013: Observations of thermally driven wind jets at the exit of Weber Canyon, Utah. *J. Appl. Meteor. Climatol.,* **52,** 1187–1200.

Colle, B. A., J. B. Wolfe, W. J. Steenburgh, D. E. Kingsmill, J. A. W. Cox, and J. C. Shafer, 2005: High-resolution simulations and microphysical validation of an orographic precipitation event over the Wasatch Mountains during IPEX IOP3. *Mon. Wea. Rev.,* **133,** 2947–2971.

Cox, J. A. W., W. J. Steenburgh, D. E. Kingsmill, J. C. Shafer, B. A. Colle, O. Bousquet, B. F. Smull, and H. Cai, 2005: The kinematic structure of a Wasatch Mountain winter storm during IPEX IOP3. *Mon. Wea. Rev.,* **133,** 521–542.

Crum, T. D., R. L. Alberty, and D. W. Burgess, 1993: Recording, archiving, and using WSR-88D data. *Bull. Amer. Meteor. Soc.,* **74,** 645–653.

Frei, C., and C. Schär, 1998: A precipitation climatology of the Alps from high-resolution rain-gauge observations. *Int. J. Climatol.,* **18,** 873–900.

Fuhrer, O., and C. Schär, 2005: Embedded cellular convection in moist flow past orography. *J. Atmos. Sci.,* **62,** 2810–2828.

——, and ——, 2007: Dynamics of orographically triggered banded convection in sheared moist orographic flows. *J. Atmos. Sci.,* **64,** 3542–3561.

Gheusi, F., and H. C. Davies, 2004: Autumnal precipitation distribution on the southern flank of the Alps: A numerical-model study of the mechanisms. *Quart. J. Roy. Meteor. Soc.,* **130,** 2125–2152.

Hill, J. D., 1971: Snow squalls in the lee of Lakes Erie and Ontario. NOAA Tech. Memo. NWS ER-43, 20 pp.

Hjelmfelt, M. R., 1990: Numerical study of the influence of environmental conditions on lake-effect snowstorms over Lake Michigan. *Mon. Wea. Rev.,* **118,** 138–150.

——, 1992: Orographic effects in simulated lake-effect snowstorms over Lake Michigan. *Mon. Wea. Rev.,* **120,** 373–377.

——, and R. R. Braham, 1983: Numerical simulation of the airflow over Lake Michigan for a major lake-effect snow event. *Mon. Wea. Rev.,* **111,** 205–219.

Hong, S.-Y., Y. Noh, and J. Dudhia, 2006: A new vertical diffusion package with an explicit treatment of entrainment processes. *Mon. Wea. Rev.,* **134,** 2318–2341.

Horel, J., and Coauthors, 2002: Mesowest: Cooperative mesonets in the western United States. *Bull. Amer. Meteor. Soc.,* **83,** 211–225.

Hozumi, K., and C. Magono, 1984: The cloud structure of convergent cloud bands over the Japan Sea in winter monsoon period. *J. Meteor. Soc. Japan,* **62,** 522–533.

Iacono, M. J., J. S. Delamere, E. J. Mlawer, M. W. Shephard, S. A. Clough, and W. D. Collins, 2008: Radiative forcing by long-lived greenhouse gases: Calculations with the AER radiative transfer models. *J. Geophys. Res.,* **113,** D13103, doi:10.1029/2008JD009944.

Jiang, Q., 2006: Precipitation over concave terrain. *J. Atmos. Sci.,* **63,** 2269–2288.

Kain, J. S., 2004: The Kain–Fritsch convective parameterization: An update. *J. Appl. Meteor.,* **43,** 170–181.

Kindap, T., 2010: A severe sea-effect snow episode over the city of Istanbul. *Nat. Hazards,* **54,** 707–723.

Kirshbaum, D. J., and D. R. Durran, 2004: Factors governing cellular convection in orographic precipitation. *J. Atmos. Sci.,* **61,** 682–698.

——, and ——, 2005a: Atmospheric factors governing banded orographic convection. *J. Atmos. Sci.,* **62,** 3758–3774.

——, and ——, 2005b: Observations and modeling of banded orographic convection. *J. Atmos. Sci.,* **62,** 1463–1479.

Kristovich, D. A. R., and N. F. Laird, 1998: Observations of widespread lake-effect cloudiness: Influences of lake surface temperature and upwind conditions. *Wea. Forecasting,* **13,** 811–821.

Kusunoki, K., M. Murakami, M. Hoshimoto, N. Orikasa, Y. Yamada, H. Mizuno, K. Hamazu, and H. Watanabe, 2004: The characteristics and evolution of orographic snow clouds under weak cold advection. *Mon. Wea. Rev.,* **132,** 174–191.

Laird, N. F., J. Desrochers, and M. Payer, 2009: Climatology of lake-effect precipitation events over Lake Champlain. *J. Appl. Meteor. Climatol.,* **48,** 232–250.

Lavoie, R. L., 1972: A mesoscale numerical model of lake-effect storms. *J. Atmos. Sci.,* **29,** 1025–1040.

Magono, C., K. Kikuchi, T. Kimura, S. Tazawa, and T. Kasai, 1966: A study on the snowfall in the winter monsoon season in Hokkaido with special reference to low land snowfall. *J. Fac. Sci. Hokkaido Univ. Ser. 7,* **11,** 287–308.

Markowski, P., and Y. Richardson, 2010: *Mesoscale Meteorology in Midlatitudes.* Wiley-Blackwell, 407 pp.

Mass, C., 1981: Orographically forced convergence in western Washington state. *Mon. Wea. Rev.,* **109,** 1335–1347.

——, and D. P. Dempsey, 1985: An orographically forced convergence line in the lee of the Olympic Mountains. *Mon. Wea. Rev.,* **113,** 659–663.

Matsuura, S., K. Matsuyama, S. Asano, T. Okamoto, and Y. Takeuchi, 2005: Fluctuation of the seasonal snowpack in a mountainous area of the heavy-snow district in the warm-temperate zone of Japan. *J. Glaciol.,* **51,** 547–554.

Mayr, G. J., and T. B. McKee, 1995: Observations of the evolution of orogenic blocking. *Mon. Wea. Rev.,* **123,** 1447–1464.

McGowan, H. A., I. F. Owens, and A. P. Sturman, 1995: Thermal and dynamic characteristics of alpine lake breezes, Lake Tekapo, New Zealand. *Bound.-Layer Meteor.,* **76,** 3–24.

Niziol, T. A., W. R. Snyder, and J. S. Waldstreicher, 1995: Winter weather forecasting throughout the eastern United States. Part IV: Lake-effect snow. *Wea. Forecasting,* **10,** 61–77.

Norris, J. G., G. Vaughan, and D. M. Schultz, 2013: Snow bands over the English Channel and Irish Sea during cold-air outbreaks. *Quart. J. Roy. Meteor. Soc.,* in press.

Onton, D. J., and W. J. Steenburgh, 2001: Diagnostic and sensitivity studies of the 7 December 1998 Great Salt Lake–effect snowstorm. *Mon. Wea. Rev.,* **129,** 1318–1338.

Passarelli, R. E., and R. R. Braham, 1981: The role of the winter land breeze in the formation of Great Lake snow storms. *Bull. Amer. Meteor. Soc.,* **62,** 482–492.

Peace, R. L., and R. B. Sykes, 1966: Mesoscale study of a lake-effect snowstorm. *Mon. Wea. Rev.,* **94,** 495–507.

Rasmussen, R., M. Dixon, S. Vasiloff, F. Hage, S. Knight, J. Vivekanandan, and M. Xu, 2003: Snow nowcasting using a real-time correlation of radar reflectivity with snow gauge accumulation. *J. Appl. Meteor.,* **42,** 20–36.

Reinking, R. F., and Coauthors, 1993: The Lake Ontario Winter Storms (LOWS) project. *Bull. Amer. Meteor. Soc.,* **74,** 1828–1849.

Richner, H., and P. Hächler, 2012: Understanding and forecasting Alpine foehn. *Mountain Weather Research and Forecasting: Recent Progress and Current Challenges,* F. K. Chow, S. F. J. de Wekker, and B. J. Snyder, Eds., Springer, 219–260.

Saito, K., M. Murakami, T. Matsuo, and H. Mizuno, 1996: Sensitivity experiments on the orographic snowfall over the mountainous region of northern Japan. *J. Meteor. Soc. Japan,* **74,** 797–813.

Schneidereit, M., and C. Schär, 2000: Idealised numerical experiments of Alpine flow regimes and south side precipitation events. *Meteor. Atmos. Phys.,* **72,** 233–250.

Sinclair, M. R., 1994: A diagnostic model for estimating orographic precipitation. *J. Appl. Meteor.,* **33,** 1163–1175.

Smith, R. B., Q. Jiang, M. G. Fearon, P. Tabary, M. Dorninger, J. D. Doyle, and R. Benoit, 2003: Orographic precipitation and air mass transformation: An Alpine example. *Quart. J. Roy. Meteor. Soc.,* **129,** 433–454.

——, I. Barstad, and L. Bonneau, 2005: Orographic precipitation and Oregon's climate transition. *J. Atmos. Sci.,* **62,** 177–191.

Splitt, M. E., and J. D. Horel, 1998: Use of multivariate linear regression for meteorological data analysis and quality assessment in complex terrain. Preprints, *10th Symp. on Meteorological Observations and Instrumentation,* Phoenix, AZ, Amer. Meteor. Soc., 359–362.

Steenburgh, W. J., 2003: One hundred inches in one hundred hours: Evolution of a Wasatch Mountain winter storm cycle. *Wea. Forecasting,* **18,** 1018–1036.

——, and T. R. Blazek, 2001: Topographic distortion of a cold front over the Snake River Plain and central Idaho mountains. *Wea. Forecasting,* **16,** 301–314.

——, and D. J. Onton, 2001: Multiscale analysis of the 7 December 1998 Great Salt Lake–effect snowstorm. *Mon. Wea. Rev.,* **129,** 1296–1317.

——, S. F. Halvorson, and D. J. Onton, 2000: Climatology of lake-effect snowstorms of the Great Salt Lake. *Mon. Wea. Rev.,* **128,** 709–727.

Stewart, J. Q., C. D. Whiteman, W. J. Steenburgh, and X. Bian, 2002: A climatological study of thermally driven wind systems of the U. S. Intermountain West. *Bull. Amer. Meteor. Soc.,* **83,** 699–708.

Thompson, G., P. R. Field, R. M. Rasmussen, and W. D. Hall, 2008: Explicit forecasts of winter precipitation using an improved bulk microphysics scheme. Part II: Implementation of a new snow parameterization. *Mon. Wea. Rev.,* **136,** 5095–5114.

Tripoli, G. J., 2005: Numerical study of the 10 January 1998 lake-effect bands observed during Lake-ICE. *J. Atmos. Sci.,* **62,** 3232–3249.

Varney, B. M., 1920: Monthly variations of the precipitation-altitude relation in the central Sierra Nevada of California. *Mon. Wea. Rev.,* **48,** 648–650.

Watson, C. D., and T. P. Lane, 2012: Sensitivities of orographic precipitation to terrain geometry and upstream conditions in idealized simulations. *J. Atmos. Sci.,* **69,** 1208–1231.

Yeager, K. N., W. J. Steenburgh, and T. I. Alcott, 2013: Contributions of lake-effect periods to the cool-season hydroclimate of the Great Salt Lake basin. *J. Appl. Meteor. Climatol.,* **52,** 341–362.